Temperature carryover effect revealed for marine fishes using spatio-temporal distributed lag models

Authors:

James T. Thorson[1], Sean C. Anderson[2,3], Max Lindmark[4]

[1] Resource Ecology and Fisheries Management Division, Alaska Fisheries Science Center, Seattle, Washington, USA

[2] Pacific Biological Station, Fisheries and Oceans Canada, Nanaimo, BC, Canada

[3] School of Resource and Environmental Management, Simon Fraser University, Burnaby, BC, Canada

[4] Swedish University of Agricultural Sciences, Department of Aquatic Resources, Sweden

* Corresponding author: James.Thorson@noaa.gov

Abstract:

Understanding the impact of changing temperature on population densities is necessary to predict the likely impact of climate anomalies (e.g., marine heatwaves) or forecast distribution shifts under future climate scenarios. Population densities are often analyzed using spatio-temporal models (STMs), which typically predict densities based on local habitat conditions while also estimating latent spatial and spatio-temporal variation. Recent research extends STMs by also estimating density responses to habitat conditions at nearby locations using a "spatially distributed lag" (SDL) that averages habitat conditions in the vicinity of samples. Here, we extend SDL by incorporating insights from diffusion-enhanced STMs to simultaneously estimate spatially distributed and time-lagged responses to nearby and past habitat conditions (a "spatio-temporal distributed lag" STDL). We then use summer bottom trawl survey data from the eastern Bering Sea (1982-2024) to measure whether spatial and/or temporal lags are parsimonious when predicting population density from temperature anomalies for six ecologically important fishes. Results show that time-lagged responses are parsimonious, positive, and substantial (correlation of 0.20-0.83 per year) for five species, and that density responses to temperature anomalies also diffuse outward over time for four species at 30-53 kilometers per year. A self- and cross-test simulation experiment shows that model selection can identify the appropriate model and parameter estimates are approximately unbiased. We therefore conclude that temperature carry-over effects arise in marine fishes and recommend that future studies include nonlocal and time-lagged responses when measuring density responses to habitat.

Keywords: Spatial distributed lag; spatio-temporal model; species distribution model; lagged response; nonlocal response

Data Availability Statement

We use records of biomass and temperature samples from the eastern Bering Sea bottom trawl surveys, described by (Markowitz *et al.*, 2022) and downloaded using release 0.0.3 of the *surveyjoin* package (Ward *et al.*, 2025) with DOI https://doi.org/10.5281/zenodo.14984411. All code required to reproduce the analysis are available publicly online at https://github.com/James-Thorson-NOAA/spacetime-lag. We will add a DOI using Zenodo upon acceptance.

Introduction

The association between animal densities and environmental variation is complicated due to nonlocal and time-lagged ecological responses. For example, migratory behaviors cause habitat conditions at one location to affect population densities at geographically distant sites, as shown by the association between local density and regional climate indices for both butterflies in California and fishes in the Bering Sea (Pardikes *et al.*, 2015; Thorson, 2019). Similarly, species interactions and age-structured dynamics result in time-lagged responses. For example, global variation in plant growth is better explained by climate indices when incorporating time-lagged responses (Wu *et al.*, 2015) due to delayed responses of the soil community in tallgrass prairie ecosystems (Arnone III *et al.*, 2008).

Species distribution models (SDMs) are widely used in ecology (Elith & Leathwick, 2009) to estimate habitat associations, attribute density changes to habitat changes, and forecast future distribution under climate scenarios (Thorson & Kristensen, 2024). Missing covariates and ecological processes (e.g., animal movement) often cause model residuals for SDMs to be correlated in space or time, and this degrades predictive performance and statistical testing (Dormann *et al.*, 2007). Recent developments in spatio-temporal generalized linear mixed models (ST-GLMMs) allow analysts to control for (and condition predictions upon) spatial and spatio-temporal autocorrelation at high spatial resolution (Thorson & Kristensen, 2024).

SDMs generally predict local densities based upon measured habitat at the same place and time and will therefore neglect the potential role of nonlocal or time-lagged responses. In past instances when SDMs are designed to test the impact of past or nonlocal environmental conditions, nonlocal and lagged effects are often tested by comparing multiple covariates at different scales in a single model, by repeatedly fitting the model with different lagged

covariates, and using model selection to identify a single spatial scale or time-lag for covariates (Wu *et al.*, 2015; Núñez-Riboni *et al.*, 2021; Lindmark *et al.*, 2023). Another option is to use SDMs to compute time-series representing range shifts, and then apply "temporal distributed lags" (TDL) to estimate the lagged effect of time-series covariates on range-shift indices (e.g., using the package *dlnm;* (Gasparrini *et al.*, 2010)). However, aggregating predictions from SDMs into an annual index reframes the analysis into a time-series framework, instead of estimating temporal lags directly within the spatially explicit SDM where spatially and temporally correlated residuals can be modelled (which *dlnm* is not designed to do). Alternatively, spatio-temporal variation in habitat covariates can be compressed to construct time-series indices representing habitat variation (e.g., using empirical orthogonal function analysis), and these indices can be included as covariates using a spatially varying response to test for nonlocal habitat responses (Thorson, 2019; Thorson *et al.*, 2020). However, this technique ignores information about the spatial proximity of habitat variation at other sites affecting local density and therefore cannot estimate the spatial- or time-scale over which nearby habitat affects local densities.

To estimate the influence of nearby habitat on population density, recent ecological research has integrated "spatially distributed lags" (SDL) into species distribution models (Miller *et al.*, 2025; Lindmark *et al.*, 2026). SDLs estimate a spatially smoothed transformation of a given covariate, and then use that transformed covariate to predict the response of a regression model (e.g., Armstrong, 2006). Similarly, ecologists are developing "temporal distributed lags" (TDL) (Sollmann, 2024; Lalechère *et al.*, 2025), and discussing the importance of both spatial and temporal lags in species distribution models (Essl *et al.*, 2024). In parallel, recent statistical research has efficiently approximated a diffusive process across space and time and used this to

96 define the distribution for a spatio-temporal latent variable (Clarotto *et al.*, 2024; Lindgren *et al.*,
97 2024). However, we are not aware of any extension re-purposing this diffusive process to define
98 a spatio-temporal distributed lag for application within a species distribution model.

99 To address this gap, we introduce a computationally efficient model to identify nonlocal
100 and/or lagged responses to habitat variables by using a "spatio-temporal distributed lag" (STDL)
101 within an SDM. To ensure that results are applicable in a wide context, we also implement this
102 while estimating spatial and spatio-temporal latent variables (e.g., using a ST-GLMM). To do so,
103 we first review recent developments in SDLs and then extend this to incorporate time-lagged
104 responses using a diffusion-enhanced process. We then demonstrate that time-lagged responses
105 to temperature anomalies arise for five of six ecologically important fishes in the eastern Bering
106 Sea, analyzed here from 1982–2024. We conclude by recommending that studies explore using
107 STDL to incorporate nonlocal and time-lagged responses to thermal habitat when testing for (or
108 forecasting) climate linkages in population distribution.

109 # Methods

110 ## Spatially distributed lags

111 We start by defining a $J \times T$ covariate matrix $\mathbf{X}$ where x_{jt} is the covariate measurement at time
112 $t \in \{1, \ldots, T\}$ and location $\mathbf{s}_j$ for $j \in \{1, \ldots, J\}$ locations in two-dimensional space within domain
113 D. We seek a spatio-temporal distributed lag operator h that transforms covariate matrix $\mathbf{X}$ to
114 calculate a transformed $J \times T$ matrix $\mathbf{Z} = h(\mathbf{X})$. We can then interpolate the covariate to
115 calculate $x_t^*(\mathbf{s}^*)$ at a new location $\mathbf{s}^*$ using a J length interpolation vector $\mathbf{a}(\mathbf{s}^*)$ where $x_t^*(\mathbf{s}^*) =$
116 $\mathbf{a}(\mathbf{s}^*)^T \mathbf{x}_t$. This operator should have the following properties:

1. *Interpretable parameters*: We seek to estimate a parameter κ_S representing the spatial distance over which a covariate is smoothed in space (e.g., units of meters) and a separate parameter κ_T representing the time-lag over which the covariate is smoothed in time (e.g., units per-year), where the model collapses to no lag in either space or time (i.e., $\mathbf{X} = \mathbf{Z}$) given some value of those parameters. We also discuss a parameter κ_{ST} that controls how a location $x_{j_1 t_1}$ affects a different location $x_{j_2 t_2}$ at a later time $t_2 > t_1$ relative to the combined effects of κ_S and κ_T (although we do not test its behavior here to simplify the presentation);
2. *Conservation of mass*: A covariate value x_{jt} at location $\mathbf{s}_j$ and time t is distributed across space and time by the STDL operator while leaving its total value (approximately) unchanged. If we define the $K \times J$ interpolation matrix $\mathbf{A}$ for K evenly distributed spatial locations $\{\mathbf{s}_1, \mathbf{s}_2, \ldots, \mathbf{s}_k\}$ within domain D, and further define $\mathbf{X}^* = \mathbf{AX}$ and $\mathbf{Z}^* = \mathbf{AZ}$, then $\sum_{t=1}^{T} \sum_{k=1}^{K} x_{kt}^* \approx \sum_{t=1}^{T} \sum_{k=1}^{K} z_{kt}^*$;
3. *Linear computation*: Using the STDL for a set of measurements $\mathbf{Z} = h(\mathbf{X})$, we seek to compute $\text{vec}(\mathbf{Z}) = \mathbf{D}^{-1}\text{vec}(\mathbf{X})$ where $\text{vec}(\mathbf{X})$ stacks the columns of $\mathbf{X}$ into a long vector with length JT, and $\mathbf{D}$ is a sparse $JT \times JT$ matrix representing the STDL which then depends upon κ_S and κ_T, such that the computation time to compute $\mathbf{D}^{-1}\text{vec}(\mathbf{X})$ increases linearly with the size of JT.

Lindmark et al. (2026) constructed a spatially distributed lag, $\mathbf{z}_t = (\mathbf{I} - \mathbf{P})^{-1}\mathbf{x}_t$ using a $J \times J$ spatial path matrix $\mathbf{P}$ given measurements $\mathbf{x}_t$ at the vertices of triangles that cover the spatial domain (a "finite element mesh" FEM). Using this FEM, $\mathbf{P} = -\kappa_s \mathbf{C}^{-1}\mathbf{G}$ where $\mathbf{C}$ is a diagonal $J \times J$ matrix measuring the volume associated with each vertex, and $\mathbf{G}$ is a sparse $J \times J$ matrix representing the "overlap" between each vertex (which is zero for vertices that do not share any triangle). However, this spatially distributed lag did not account for time-lags and therefore

could not assess the relative importance of temporal versus spatial lags. We therefore seek to extend this recent research to also include time-lags.

Extending to include time-lags

We next incorporate time-lagged dynamics, where covariate measurements $\mathbf{x}_t$ affect the STDL covariate $\mathbf{z}_t$ in that same time but also in future times $\mathbf{z}_{t+1}$, $\mathbf{z}_{t+2}$, etc. To do so, we construct a $JT \times JT$ dimensional path matrix $\mathbf{P}_{\text{joint}}$ from spatial, temporal, and spatio-temporal lags:

$$\mathbf{P}_{\text{joint}} = \underbrace{\kappa_S^{-2}(\mathbf{P} \otimes \mathbf{I}_T)}_{\text{Space lag}} + \underbrace{\kappa_T(\mathbf{I}_S \otimes \mathbf{L})}_{\text{Time lag}} + \underbrace{\kappa_{ST}\kappa_S^{-2}(\mathbf{P} \otimes \mathbf{L})}_{\text{Space-time lag}}, \quad (1)$$

where $\mathbf{L}$ is a $T \times T$ first-difference matrix (with a band of 1s immediately below the diagonal and a band of -1s along the diagonal), $\mathbf{I}_T$ is a $T \times T$ identity matrix, $\mathbf{I}_S$ is a $J \times J$ identity matrix, and $-1 < \kappa_{ST} < 0$ controls the rate at which x_{jt} diffuses outward over time (with no diffusion when $\kappa_{ST} = -1$). To simplify presentation in the following, however, we drop the space-time lag (i.e., fix $\kappa_{ST} = 0$) and only estimate κ_S and κ_T. The STDL operator then calculates $\text{vec}(\mathbf{z}) = \left(\mathbf{I} - \mathbf{P}_{\text{joint}}\right)^{-1}\text{vec}(\mathbf{x})$ and $\text{vec}(\mathbf{z})$ can be computed from $\mathbf{I} - \mathbf{P}_{\text{joint}}$ using a sparse LU decomposition (Rue & Held, 2005) without directly constructing $\left(\mathbf{I} - \mathbf{P}_{\text{joint}}\right)^{-1}$.

This expression results in a linear increase in mean-squared displacement (MSD) over time (i.e., the effect of a covariate x_{jt} propagates outwards spatially over time), and an exponential decay in the covariate effect over time. Specifically, it results in a first-order autocorrelation time ϕ:

$$\phi = \frac{\kappa_T}{1 + \kappa_T}, \quad (2)$$

and a mean-squared displacement (MSD) for the covariate:

$$\text{MSD} = 4\kappa_S^{-2}(1-\phi) = \frac{4\kappa_S^{-2}}{1+\kappa_T}, \quad (3)$$

which we will visualize in detail later.

Carry-over effects for temperature anomalies in the eastern Bering Sea

To demonstrate nonlocal and/or lagged responses to habitat variables, we fit a species distribution model to bottom trawl samples of fish biomass in the eastern Bering Sea. The trawl survey was conducted following a fixed-station design with 291 to 376 stations over a 493,894.5 km^2 spatial domain from 1982 to 2019 and 2021 to 2024 (Markowitz *et al.*, 2022) and downloaded using the *surveyjoin* package (Ward *et al.*, 2025). We specifically fit a separate spatio-temporal generalized linear mixed model (ST-GLMM) to biomass y_i using area swept w_i as an offset for each of six ecologically important species: Pacific cod (*Gadus macrocephalus*), Alaska pollock (*Gadus chalcogrammus*), capelin (*Mallotus villosus*), herring (*Clupea pallasii*), arrowtooth flounder (*Atheresthes stomias*), and Pacific halibut (*Hippoglossus stenolepis*) (Thorson & Kristensen, 2024). We specify a Tweedie distribution:

$$y_i \sim \text{Tweedie}(\mu_i, \phi, \psi) \quad (4)$$

which involves estimating two dispersion parameters that control the mean-variance relationship $\text{Var}(y_i) = \phi\mu_i^{\psi}$. The mean is then predicted from a log-linked linear predictor:

$$\log(\mu_i) = \underbrace{\beta}_{\text{Intercept}} + \underbrace{\omega_{j[i]}}_{\substack{\text{Spatial} \\ \text{term}}} + \underbrace{\epsilon_{j[i],t[i]}}_{\substack{\text{Spatio-temporal} \\ \text{Term}}} + \underbrace{\gamma_1 z_{j[i],t[i]} + \gamma_1 z^2_{j[i],t[i]}}_{\substack{\text{Quadratic effect of} \\ \text{spatio-temporal distributed lag} \\ \text{for temperature}}} + \underbrace{\log(w_i)}_{\text{Area offset}} \quad (5)$$

We specify a Gaussian Markov random field (GMRF) for the spatial term:

$$\boldsymbol{\omega} \sim \text{GMRF}(\mathbf{0}, \tau_\omega^2 \mathbf{Q}), \quad (6)$$

where $\mathbf{Q}$ is the sparse precision matrix constructed using the SPDE method (Lindgren *et al.*, 2011), and also specify a GMRF that follows a first-order autoregressive process for the spatio-temporal term:

$$\boldsymbol{\epsilon}_t \sim \begin{cases} \text{GMRF}(\mathbf{0}, (1-\rho_\epsilon^2)\tau_\epsilon^2\mathbf{Q}) & \text{if } t = 1 \\ \text{GMRF}(\rho_\epsilon \boldsymbol{\epsilon}_t, \tau_\epsilon^2\mathbf{Q}) & \text{if } t > 1 \end{cases}. \quad (7)$$

This involves estimating the decorrelation rate κ that is shared between spatial and spatio-temporal terms, the time-correlation ρ_ϵ for spatio-temporal residuals, and a separate pointwise variance for each term controlled by τ_ω^2 and τ_ϵ^2, respectively. The SPDE method requires constructing a finite-element mesh (FEM) over the spatial domain, which we do using the *fmesher* package (Lindgren, 2023). We use a FEM cutoff of 30 km, resulting in $J = 402$ vertices over $T = 45$ years, such that $\boldsymbol{\omega}$ and $\boldsymbol{\epsilon}_t$ contain 18,492 random effects.

Finally, we also estimate κ_S and κ_T for the STDL that converts seafloor temperature anomalies x_{jt} to effective covariate z_{jt}, while then estimating a dome-shaped (quadratic) response to z_{jt}. We use *in situ* measurements of water temperature obtained from the bottom trawl survey to define the seafloor temperature x_{jt} for each vertex j of the SPDE mesh at location $\mathbf{s}_j$ in year t, using the nearest bottom trawl sample to $\mathbf{s}_j$ in a given year. Because the survey was not conducted in 2020, we estimated bottom temperature for that year by averaging observations from the two adjacent survey years, 2019 and 2021. To allow a time-lagged effect of past temperatures for the first year of sampling, we imputed the 1981 values using the mean of 1982-1983. We then convert the bottom temperature for a given location j and year t to a temperature anomaly by subtracting the mean value for that location across years. This temperature anomaly shows a well-documented oscillation (Stabeno *et al.*, 2019) between a

193 warm stanza (2002 to 2005), a cold stanza (2006 to 2013), another warm stanza (2014 to 2021),
194 with close-to-average conditions subsequently (Fig. 1).

195 For each species, we fit four models formed from the 2×2 factorial design of including
196 the space-lag by estimating κ_S (or instead fixing $\kappa_S = 0$) and/or including the time-lag by
197 estimating κ_T (or instead fixing $\kappa_T = 0$). For each model, we identify the maximum likelihood
198 estimate of all fixed effects by applying the Laplace approximation to the joint likelihood of
199 fixed and random effects (Skaug & Fournier, 2006), as implemented using the R (R Core Team,
200 2023) package *TMB* (Kristensen *et al.*, 2016). TMB then calculates the gradient of the Laplace
201 approximation with respect to fixed effects using automatic differentiation (Fournier *et al.*,
202 2012), which we then optimize in the R statistical environment. TMB uses the Eigen package
203 (Guennebaud *et al.*, 2010) to efficiently apply the sparse LU decomposition when calculating the
204 STDL, and we use the delta method to compute standard errors for ϕ (Eq. 2), MSD (Eq. 3), and
205 $\mathrm{RMSD} = \sqrt{\mathrm{MSD}}$.

206 We explore model results in several ways:

207 1. *Parsimony and parameter estimates*: For each species, we calculate the Akaike Information
208 Criterion (AIC) (Akaike, 1974) and use it to identify the most parsimonious of the four
209 models. For all four models, we also extract the estimated spatial distributed lag (κ_S) and the
210 temporal distributed lag (κ_T), and convert them to the equivalent mean-squared displacement
211 MSD and the first-order autocorrelation ϕ, respectively. We then compare the ϕ and MSD
212 across species and models.
213 2. *Visualized effect of temperature anomalies*: For the selected model for each species, we also
214 visualize the predicted effect of a hypothetical anomaly in local temperature as it propagates

through space and time, based on the estimated values of κ_S and κ_T. This plot provides intuition about the spatial and temporal scale over which a temperature anomaly affects population density for that species.

3. *Effective seafloor temperature*: Finally, for the selected model for each species, we also visualize the effective seafloor temperature $\mathbf{Z}^*$ after applying the STDL to the *in situ* measurements $\mathbf{X}$ and then interpolating $\mathbf{Z}$ to the 25 km × 25 km grid. This effective temperature then represents the net effective of animal movement and carryover effects that contribute to the estimated STDL.

Both (2) and (3) involve predicting raw covariate $\mathbf{X}$ and the STDL covariate $\mathbf{Z}$ at higher resolution. To do so we construct a set of $K = 886$ square 25 km × 25 km grid cells that cover the spatial domain of the bottom trawl survey, and then interpolate covariates $\mathbf{X}^* = \mathbf{AX}$ and $\mathbf{Z}^* = \mathbf{AZ}$ using the $K \times J$ interpolation matrix $\mathbf{A}$.

Simulation experiment

To explore model performance, we conduct a self- and cross-test simulation experiment assessing parameter recovery and whether AIC correctly identifies the true model across different estimation scenarios. To do so, we choose three species where model selection for real data selects either no STDL (Pacific cod), a temporal lag (Pacific halibut), or both spatial and temporal lags (capelin). For each species, we simulate 100 replicated data sets from the AIC-selected model (used as operating model), each of which condition upon the maximum likelihood estimates for fixed effects, simulating new realizations of the random effects, and then simulating new samples conditional upon both at the same location as real-world data. For each of 100 data sets, we then fit the original four estimation models: no lags, spatial lag, time-lag,

and both space and time lags (1200 model fits) and record the AIC and parameter estimates. We then explore (1) how often AIC identifies the correct data-generating process, and (2) how the estimated parameters compare with the original values used in the simulation.

Results

The most parsimonious model (lowest marginal AIC) includes a carry-over effect of temperature for five of the six species (Table 1). For these five species, the AIC-selected model has a temporal correlation ϕ from ranging from 0.20 (arrowtooth flounder) to 0.83 (Pacific herring). Similarly, the spatial lag is parsimonious for four of the six species and has a root-mean-squared displacement (RMSD) ranging from 30 km (arrowtooth flounder) to 53 km (capelin), relative to the $\sqrt{493{,}894.5} = 703$ km distance across the spatial domain. Models without the STDL run in 3.2 to 11.2 minutes and adding the STDL increases runtime by 5-fold to 15-fold. As expected, the selected model has a 95% confidence interval for ϕ and RMSD that does not overlap with zero when AIC favors a model with STDL, and the interval generally does overlap zero when the component is not selected by AIC (Fig. 2); for example Pacific cod where $\phi = 0.04$ and is not selected as parsimonious.

To illustrate the predicted effect of the estimated spatial and time-lags, we illustrate how a hypothetical localized temperature anomaly propagates across space and over time (Fig. 3). Pacific cod (Fig. 3 top row) is the only species where AIC selects neither the time- or nor space-lags. For this species, the local temperature anomaly $\mathbf{X}_t^*$ has a mean-squared displacement of MSD $= 911$ km^2, i.e., RMSD $= \sqrt{911} = 30$ km. This matches the scale used when discretizing the continuous covariate (i.e., 40 km cutoff in the finite-element mesh), such that the resolution of the finite element mesh provides a "lower bound" on the spatial resolution of the simulated

local temperature anomaly $\mathbf{X}_t^*$. The diffused covariate $\mathbf{Z}_t^*$ then has the same total value and MSD in that year, and $\mathbf{Z}_{t+1}^* = 0$ in subsequent years (shown as dark blue in lag-1 and lag-2 columns) because there is no time-lagged dynamics ($\kappa_T = 0$). By contrast, Pacific halibut selects a time-lag but no spatial lag (Fig. 3, bottom row), with $\phi = 0.31$. As a result, the covariate is smoothed across years, where the total effect in the first three years is 0.69, 0.22, and 0.07 (i.e., $\frac{0.22}{0.69} = 0.31$), and the sum across all subsequent years is approximately 1 (i.e., the total effect of a temperature anomaly is preserved but smoothed across subsequent years). However, the spatial lag is not selected, such that the spatial effect does not propagate outward over time (MSD = 978 km^2 in all years). As a third example, walleye pollock (Fig. 3, 2nd row) selects both a time and space lag, with estimated MSD = 1747 km^2 and $\phi = 0.31$ In this case, the effect of a temperature anomaly propagates outwards over time, i.e., MSD = 2621 km^2 in the initial year and MSD = 4294 km^2 in the following year.

The STDL estimates substantial differences in the effective temperature anomaly $\mathbf{Z}^*$ among species, and we use the transition from cold (2013) to warm (2017) conditions as an illustrative example (Fig. 4). For Pacific cod, AIC selects the model without any space or time-lag, and therefore effective temperature (Fig. 4 top row) is identical to the raw measurements (Fig. 1). As an extreme contrast, the selected model for Pacific herring has strong spatial and time-lags (RMSD = 46 km and $\phi = 0.84$), so effective temperature shows both less variation across space within a year and also a slower transition from below- (blue) to above-average (red) conditions starting in 2016 (Fig. 4, 4th row). Using Pacific halibut as an example that includes time-lags but no spatial lag ($\phi = 0.31$), we see the same high-resolution spatial variation in effective temperature as for measurements (Fig. 1) and for Pacific cod (Fig. 1 top row), but the persistence of below-average effective temperature across the northern portion of the survey area

even as temperature measurements are increasing in 2014. We therefore see that STDL estimates the effective thermal environment, which can differ from raw measurements and among species.

Finally, the simulation experiment confirms that AIC can identify the combination of spatial and temporal distributed lags that are used to simulate data (Fig. 5). In particular, the correct model is identified in >75% of simulation replicates for all three species. Similarly, the estimates of spatio-temporal lags are approximately unbiased for those cases where they are simulated (Fig. 6). We therefore conclude that these parameters are estimable given the sample sizes explored here.

Discussion

In this paper, we provide the first demonstration that both temporal and high-resolution spatial lags arise when using habitat variables (e.g., temperature anomalies) to predict population density. The method involves estimating two additional, interpretable parameters (i.e., with units of distance and time), and the spatio-temporal distributed lag can revert to the conventional species distribution model (i.e., using measured covariates directly) as a nested submodel. Similarly, a simulation experiment suggests that model selection can identify the appropriate combination of spatial and temporal lags, and that estimates are approximately unbiased using the sample sizes explored here. The estimated temporal lags are strongest for the two pelagic species (Pacific herring and capelin have $\phi = \{0.83, 0.70\}$), and either weak or absent for two seafloor-associated species (Pacific halibut and Pacific cod have $\phi = \{0.31, 0.04\}$). The method also allows us to visualize the effective temperature anomaly for each fish population, which differs substantially among species.

303 The link between spatio-temporal distributed lags (Eq. 1) and animal movement suggests
304 many avenues for future extensions to this approach. We did not explore estimating the spatio-
305 temporal interaction κ_{ST} so that we could focus on two interpretable parameters. However,
306 estimating κ_{ST} allows the STDL to estimate a separate RMSD in the first year relative to how
307 much RMSD increases in subsequent years; $\kappa_{ST} = 0$ (as assumed here) results in MSD increasing
308 linearly with time, whereas $\kappa_{ST} = -1$ results in MSD being equal for all years. This parameter
309 therefore allows a model to estimate the rate of spatio-temporal diffusion, at the cost of slower
310 model fitting. Similarly, the spatial diffusion rate κ_S might itself depend upon covariates
311 (Lindgren *et al.*, 2011), where temperature anomalies might have a more localized impact on
312 nearshore than deep-water habitats. Future studies could incorporate this novel type of covariate
313 interaction during the construction of stiffness matrix $\mathbf{G}$. Finally, including advection would
314 allow covariates at one location to affect population responses some distance away (e.g., 100 km
315 eastward). For an animal with predictable seasonal movement, this would allow winter
316 covariates to affect summer densities at a geographically distant site.

317 Oceans are experiencing extremely warm conditions (Hobday *et al.*, 2016), and there are
318 well-documented examples of marine heatwaves impacting ocean animals (Fossheim *et al.*,
319 2015; Szuwalski *et al.*, 2023). However, a global synthesis (Fredston *et al.*, 2023) found no
320 consistent change in region-wide seafloor-community biomass occurring synchronous with
321 marine heatwaves. We hypothesize that this mismatch arises because spatial and temporal lags
322 can complicate studies seeking to attribute ecological responses to climate drivers. In cases such
323 as this, we hypothesize that the STDL allows analysts to attribute localized density responses to
324 temperature anomalies, while automatically testing for lagged responses and identifying the
325 appropriate scale linking temperature to population responses. We therefore recommend greater

use of STDL in studies attributing ecological dynamics to climate drivers, and the growing availability of global databases of biological monitoring (Maureaud *et al.*, 2024) will facilitate these studies.

Acknowledgements

We thank Jon Reum, Maurice Goodman, and Paul Van Dam Bates for helpful comments on an earlier draft.

References

Akaike H (1974) New look at statistical-model identification. *IEEE Transactions on Automatic Control*, **AC19**, 716–723.

Armstrong B (2006) Models for the Relationship between Ambient Temperature and Daily Mortality. *Epidemiology*, **17**, 624–631.

Arnone III JA, Verburg PSJ, Johnson DW et al. (2008) Prolonged suppression of ecosystem carbon dioxide uptake after an anomalously warm year. *Nature*, **455**, 383–386.

Clarotto L, Allard D, Romary T, Desassis N (2024) The SPDE approach for spatio-temporal datasets with advection and diffusion. *Spatial Statistics*, **62**, 100847.

Dormann C, McPherson J, Araújo M et al. (2007) Methods to account for spatial autocorrelation in the analysis of species distributional data: a review. *Ecography*, **30**, 609–628.

Elith J, Leathwick JR (2009) Species distribution models: ecological explanation and prediction across space and time. *Annual review of ecology, evolution, and systematics*, **40**, 677–697.

Essl F, García-Rodríguez A, Lenzner B et al. (2024) Potential sources of time lags in calibrating species distribution models. *Journal of Biogeography*, **51**, 89–102.

Fossheim M, Primicerio R, Johannesen E, Ingvaldsen RB, Aschan MM, Dolgov AV (2015) Recent warming leads to a rapid borealization of fish communities in the Arctic. *Nature Climate Change*, **5**, 673–677.

Fournier DA, Skaug HJ, Ancheta J et al. (2012) AD Model Builder: using automatic differentiation for statistical inference of highly parameterized complex nonlinear models. *Optimization Methods and Software*, **27**, 1–17.

Fredston AL, Cheung WW, Frölicher TL et al. (2023) Marine heatwaves are not a dominant driver of change in demersal fishes. *Nature*, **621**, 324–329.

Gasparrini A, Armstrong B, Kenward MG (2010) Distributed lag non-linear models. *Statistics in Medicine*, **29**, 2224–2234.

Guennebaud G, Jacob B, others (2010) Eigen v3.

Hobday AJ, Alexander LV, Perkins SE et al. (2016) A hierarchical approach to defining marine heatwaves. *Progress in Oceanography*, **141**, 227–238.

Kristensen K, Nielsen A, Berg CW, Skaug H, Bell BM (2016) TMB: Automatic differentiation and Laplace approximation. *Journal of Statistical Software*, **70**, 1–21.

Lalechère E, Marrec R, Lenoir J (2025) A Non-Equilibrium Species Distribution Model Reveals Unprecedented Depth of Time Lag Responses to Past Environmental Change Trajectories. *Ecology Letters*, **28**, e70040.

Lindgren F (2023) fmesher: Triangle Meshes and Related Geometry Tools.

Lindgren F, Rue H, Lindström J (2011) An explicit link between Gaussian fields and Gaussian Markov random fields: the stochastic partial differential equation approach. *Journal of the Royal Statistical Society: Series B (Statistical Methodology)*, **73**, 423–498.

Lindgren F, Bakka H, Bolin D, Krainski E, Rue H (2024) A diffusion-based spatio-temporal extension of Gaussian Matérn fields. *Statistics and Operations Research Transactions (SORT)*, **48**, 3–66.

Lindmark M, Anderson SC, Gogina M, Casini M (2023) Evaluating drivers of spatiotemporal variability in individual condition of a bottom-associated marine fish, Atlantic cod (Gadus morhua). *ICES Journal of Marine Science*, **80**, 1539–1550.

Lindmark M, Anderson SC, Thorson JT (2026) Estimating scale-dependent covariate responses using two-dimensional diffusion derived from the stochastic partial differential equation method. *Methods in Ecology and Evolution*, **17**, 207–218.

Markowitz EH, Dawson EJ, Charriere NE, Prohaska BK, Rohan SK, Stevenson DE, Britt LL (2022) Results of the 2021 eastern and northern Bering Sea continental shelf bottom trawl survey of groundfish and invertebrate fauna.

Maureaud AA, Palacios-Abrantes J, Kitchel Z et al. (2024) FISHGLOB_data: an integrated dataset of fish biodiversity sampled with scientific bottom-trawl surveys. *Scientific Data*, **11**, 24.

Miller DL, Newman K, Cornulier T (2025) Adding structure to generalized additive models, with applications in ecology.

Núñez-Riboni I, Akimova A, Sell AF (2021) Effect of data spatial scale on the performance of fish habitat models. *Fish and Fisheries*, **22**, 955–973.

Pardikes NA, Shapiro AM, Dyer LA, Forister ML (2015) Global weather and local butterflies: variable responses to a large-scale climate pattern along an elevational gradient. *Ecology*, **96**, 2891–2901.

R Core Team (2023) *R: A Language and Environment for Statistical Computing*. R Foundation for Statistical Computing, Vienna, Austria.

Rue H, Held L (2005) *Gaussian Markov random fields: theory and applications*, 1st edition edn. CRC Press, 280 pp.

Skaug H, Fournier D (2006) Automatic approximation of the marginal likelihood in non-Gaussian hierarchical models. *Computational Statistics & Data Analysis*, **51**, 699–709.

Sollmann R (2024) Estimating the temporal scale of lagged responses in species abundance and occurrence. *Ecosphere*, **15**, e4704.

Stabeno PJ, Bell SW, Bond NA, Kimmel DG, Mordy CW, Sullivan ME (2019) Distributed Biological Observatory Region 1: Physics, chemistry and plankton in the northern Bering Sea. *Deep Sea Research Part II: Topical Studies in Oceanography*, **162**, 8–21.

Szuwalski CS, Aydin K, Fedewa EJ, Garber-Yonts B, Litzow MA (2023) The collapse of eastern Bering Sea snow crab. *Science*, **382**, 306–310.

Thorson JT (2019) Measuring the impact of oceanographic indices on species distribution shifts: The spatially varying effect of cold-pool extent in the eastern Bering Sea. *Limnology and Oceanography*, **64**, 2632–2645.

Thorson J, Kristensen K (2024) *Spatio-Temporal Models for Ecologists*, 1st edition edn. Chapman and Hall/CRC, Boca Raton, FL, 276 pp.

Thorson JT, Ciannelli L, Litzow MA (2020) Defining indices of ecosystem variability using biological samples of fish communities: A generalization of empirical orthogonal functions. *Progress in Oceanography*, **181**, 102244.

Ward EJ, English PA, Rooper CN et al. (2025) 'surveyjoin': A Standardized Database of Fisheries Bottom Trawl Surveys in the Northeast Pacific Ocean. 2025.03.14.643022.

Wu D, Zhao X, Liang S, Zhou T, Huang K, Tang B, Zhao W (2015) Time-lag effects of global vegetation responses to climate change. *Global Change Biology*, **21**, 3520–3531.

Table 1 – Summary of model results for the six species and four models formed from the 2×2 cross of including a space lag (X in space column) or time lag (X in time-lag). We specifically show the runtime in minutes (including optimization from uniformed starting values and standard-error calculations), the marginal AIC relative to the most parsimonious model (in bold for selected model), the first-order autocorrelation ϕ calculated from estimated time-lag κ_T (Eq. 2), the mean-squared displacement MSD calculated from the space-lag κ_S (Eq. 3), and the square-root of MSD (with units of km)

Species (common name)	space	time	Runtime (min)	ΔAIC	ϕ	MSD (km^2)	RMSD (km)
pacific cod			**3.24**	**0**	**NA**	**NA**	**NA**
pacific cod	X		3.85	2	NA	0	0
pacific cod		X	4.87	1.5	0.04	NA	NA
pacific cod	X	X	17.35	3.5	0.04	0	0
walleye pollock			3.42	2.55	NA	NA	NA
walleye pollock	X		4.28	3.28	NA	664	26
walleye pollock		X	3.71	2.21	0.16	NA	NA
walleye pollock	**X**	**X**	**15.37**	**0**	**0.31**	**1747**	**42**
capelin			3.31	21.88	NA	NA	NA
capelin	X		5.1	11.1	NA	5072	71
capelin		X	3.56	10.3	0.52	NA	NA
capelin	**X**	**X**	**29.73**	**0**	**0.7**	**2804**	**53**
pacific herring			8.19	10.26	NA	NA	NA
pacific herring	X		10.32	12.26	NA	0	0
pacific herring		X	8.79	3.51	0.73	NA	NA
pacific herring	**X**	**X**	**29.26**	**0**	**0.83**	**2135**	**46**
arrowtooth flounder			6.77	6.12	NA	NA	NA
arrowtooth flounder	X		8.63	2.87	NA	912	30
arrowtooth flounder		X	9.84	3.14	0.18	NA	NA
arrowtooth flounder	**X**	**X**	**32.26**	**0**	**0.2**	**911**	**30**
pacific halibut			11.15	9.58	NA	NA	NA
pacific halibut	X		4.62	11.58	NA	0	0
pacific halibut		**X**	**2.89**	**0**	**0.31**	**NA**	**NA**
pacific halibut	X	X	11.87	2	0.31	0	0

Fig. 1 – Visualizing temperature anomalies $\mathbf{X}^*$ (see panel 1981 for color legend) interpolated to the 40 × 40 km grid cells distributed across the eastern Bering Sea survey area (black outline) relative to land in Alaska (grey areas) from 1981 to 2024 (panels).

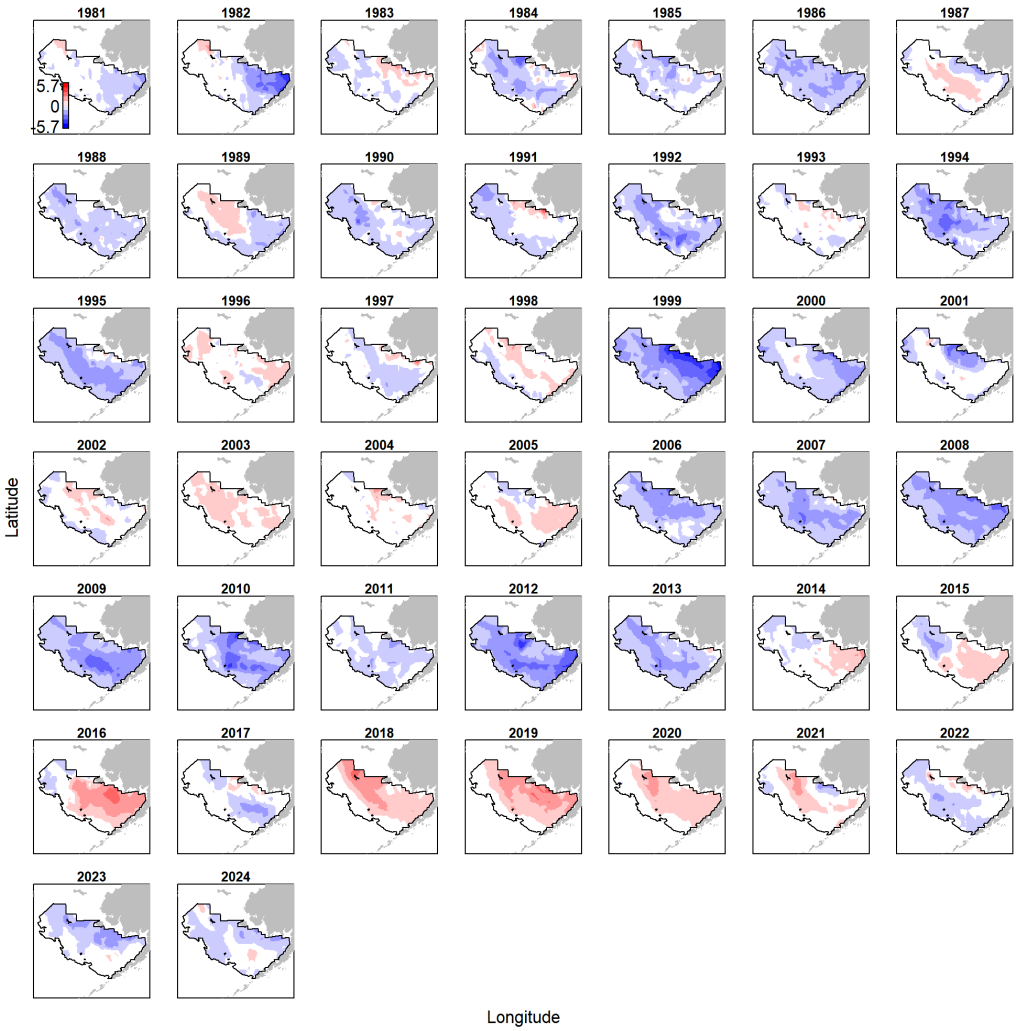

Fig. 2 – Visualizing estimated AIC weight (top row), the correlation among years (2nd row), and the root-mean-squared displacement (3rd row) for the spatio-temporal distributed lag for each of four models (x-axis; null: no lags; S: just spatial lag; T: just time-lag; ST: both space and time lags) for each of six species (columns)

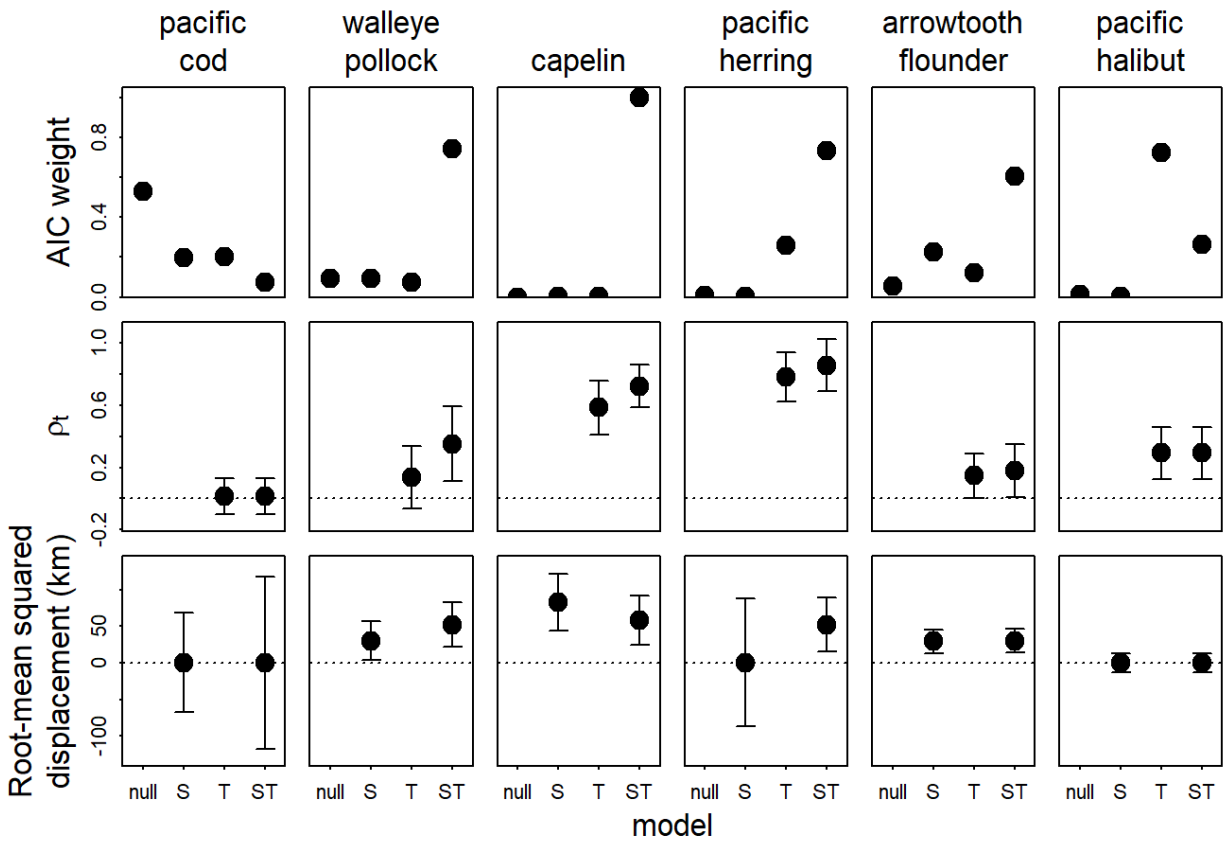

Fig. 3 – Using the selected model for each species (row), visualizing the effect of a hypothetical, localized temperature anomaly measurement $\mathbf{x}_t^*$ interpolated to the 40 km × 40 km grid cells (left column), and how it translates to the effective temperature in the same year $\mathbf{z}_t^*$ (2nd column), one year later $\mathbf{z}_{t+1}^*$ (3rd column), or two years later $\mathbf{z}_{t+2}^*$ (4th column). We specifically fix $x_{jt} = c$ for the location $\mathbf{s}_j$ in the middle of the spatial domain, with value c fixed to ensure that $\sum_{k=1}^{K} x_{kt}^* = 1$, where k is the number of grid cells. For each year, we calculate the total $\sum_{k=1}^{K} x_{kt}^*$ or $\sum_{k=1}^{K} z_{kt}^*$ and the root-mean-squared displacement (listed above each panel). We also show the edges of the set of triangles (grey lines) used to represent the finite-element mesh (using a cutoff of 40 km).

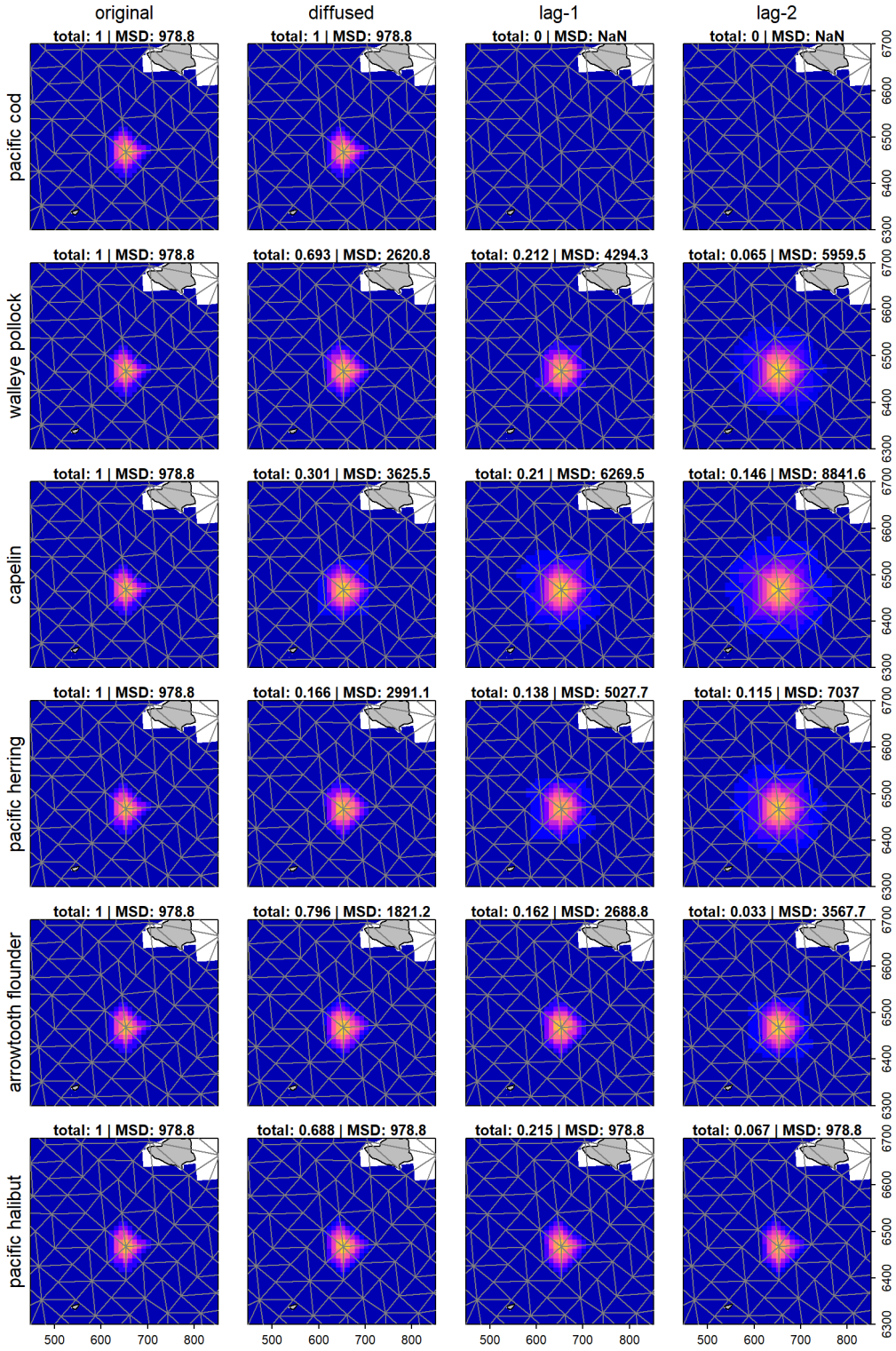
original
diffused
lag-1
lag-2
pacific cod
walleye pollock
capelin
pacific herring
arrowtooth flounder
pacific halibut
total: 1 | MSD: 978.8
total: 1 | MSD: 978.8
total: 0 | MSD: NaN
total: 0 | MSD: NaN
total: 1 | MSD: 978.8
total: 0.693 | MSD: 2620.8
total: 0.212 | MSD: 4294.3
total: 0.065 | MSD: 5959.5
total: 1 | MSD: 978.8
total: 0.301 | MSD: 3625.5
total: 0.21 | MSD: 6269.5
total: 0.146 | MSD: 8841.6
total: 1 | MSD: 978.8
total: 0.166 | MSD: 2991.1
total: 0.138 | MSD: 5027.7
total: 0.115 | MSD: 7037
total: 1 | MSD: 978.8
total: 0.796 | MSD: 1821.2
total: 0.162 | MSD: 2688.8
total: 0.033 | MSD: 3567.7
total: 1 | MSD: 978.8
total: 0.688 | MSD: 978.8
total: 0.215 | MSD: 978.8
total: 0.067 | MSD: 978.8
500
600
700
800
6300
6400
6500
6600
6700

Fig. 4 – Visualizing the effective seafloor temperature anomaly $\mathbf{z}_t^*$ (in units ℃ relative to the average for 1982-2014) for each species (rows) in the five years that rapidly transition from cool (2013, left column) to warm conditions (2017, right column), and using a separate color legend for each species (within the left panel for each row); compare with Fig. 1 to see the effect of the spatio-temporal distributed lag.

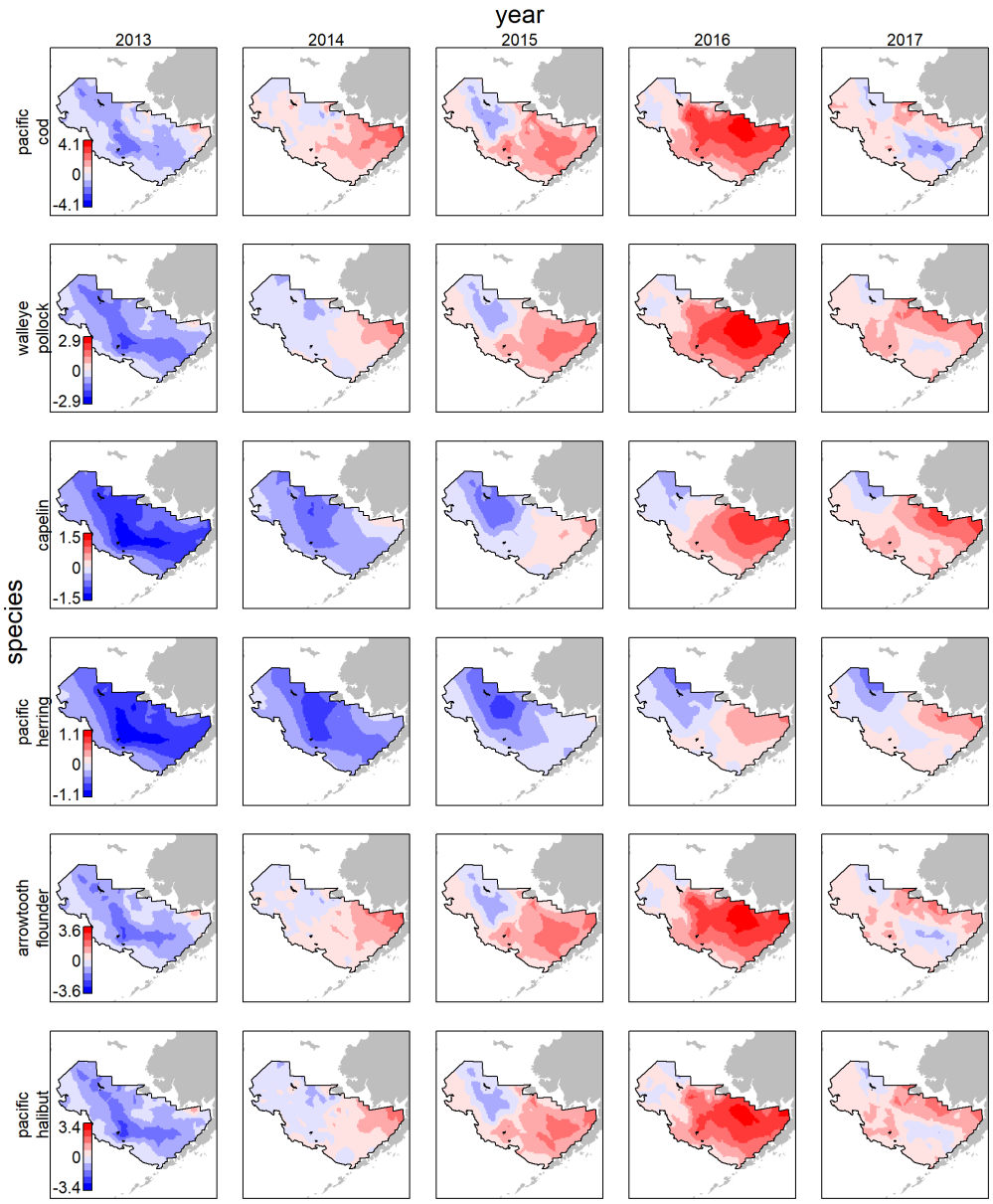

Fig. 5 – Performance for marginal AIC to identify the correct model within a simulation experiment for three species. For each species (columns), we show the four estimation models (x-axis; null: no lags; S: just spatial lag; T: just time-lag; ST: both space and time lags), and the proportion of 100 simulation replicates where each model was selected (y-axis). Color corresponds to whether the operating model matches the estimation model, where green matches (correct model is chosen) and orange is a mismatch (incorrect model chosen).

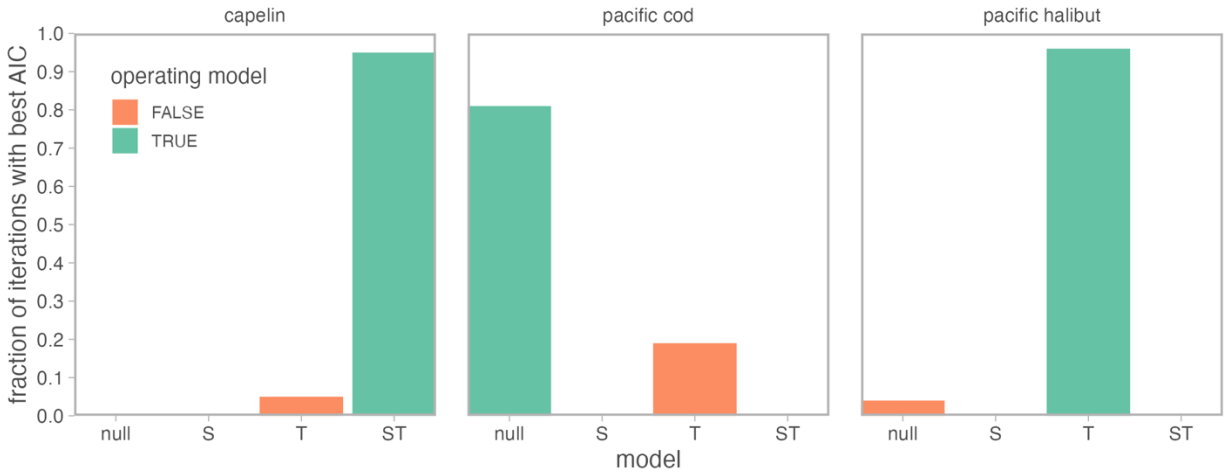

Fig. 6 – Performance of parameter estimation in the simulation experiment, showing the two parameters in the spatio-temporal distributed lag for capelin (panel A and B) and the temporal lag for Pacific halibut (panel C), as well as the derived calculation for root-mean-squared-displacement in km (RMSD) (panel D) and correlation among years (autocorrelation) (panel E and F). For each quantity, we show 100 estimates (dots) and the true value (red line; y-axis) for the two estimation models, where green indicates the operating model and orange indicates the alternative model that also estimates the same parameter (x-axis; S: just spatial lag; T: just time-lag; ST: both space and time lags). Estimates where RMSD < 1 are shown as crosses.